

Infrared photodissociation of a water molecule from a flexible molecule-H₂O complex: Rates and conformational product yields following XH stretch excitation

Jasper R. Clarkson

Department of Chemistry, Purdue University, West Lafayette, Indiana 47907

John M. Herbert

Department of Chemistry, The Ohio State University, Columbus, Ohio 43210

Timothy S. Zwier^{a)}

Department of Chemistry, Purdue University, West Lafayette, Indiana 47907

(Received 8 November 2006; accepted 7 February 2007; published online 3 April 2007)

Infrared-ultraviolet hole-burning and hole-filling spectroscopies have been used to study IR-induced dissociation of the tryptamine·H₂O and tryptamine·D₂O complexes. Upon complexation of a single water molecule, the seven conformational isomers of tryptamine collapse to a single structure that retains the same ethylamine side chain conformation present in the most highly populated conformer of tryptamine monomer. Infrared excitation of the tryptamine·H₂O complex was carried out using a series of infrared absorptions spanning the range of 2470–3715 cm⁻¹. The authors have determined the conformational product yield over this range and the dissociation rate near threshold, where it is slow enough to be measured by our methods. The observed threshold for dissociation occurred at 2872 cm⁻¹ in tryptamine·H₂O and at 2869 cm⁻¹ in tryptamine·D₂O, with no dissociation occurring on the time scale of the experiment (~2 μs) at 2745 cm⁻¹. The dissociation time constants varied from ~200 ns for the 2869 cm⁻¹ band of tryptamine·D₂O to ~25 ns for the 2872 cm⁻¹ band of tryptamine·H₂O. This large isotope dependence is associated with a zero-point energy effect that increases the binding energy of the deuterated complex by ~190 cm⁻¹, thereby reducing the excess energy available at the same excitation energy. At all higher energies, the dissociation lifetime was shorter than the pulse duration of our lasers (8 ns). At all wavelengths, the observed products in the presence of collisions are dominated by conformers A and B of tryptamine monomer, with small contributions from the other minor conformers. In addition, right at threshold (2869 cm⁻¹), tryptamine·D₂O dissociates exclusively to conformer A in the absence of collisions with helium, while both A and B conformational products are observed in the presence of collisions with helium. Using resolution-of-identity approximation to second-order Møller-Plesset binding energies extrapolated to the complete basis set limit and harmonic vibrational frequencies and transition states calculated at the density functional limit B3LYP/6-31+G* level of theory, Rice-Ramsperger-Kassel-Marcus (RRKM) predictions for the dissociation, isomerization, and water shuttling rates as a function of energy are made. At threshold, the experimental dissociation rate is almost 10³ faster than RRKM predictions. Reasons for this apparent non-RRKM behavior will be discussed. © 2007 American Institute of Physics. [DOI: 10.1063/1.2713109]

I. INTRODUCTION

In solution, conformational isomerization of a flexible molecule necessarily occurs by an intimate exchange of energy with the solvent, affecting the rates of isomerization and the pathways taken from reactant to product. This competition and influence are echoed already in the dissociation dynamics of a flexible biomolecule-H₂O complex. The full potential energy surface for such a complex is a complicated one, containing minima associated with the various conformational isomers of the flexible biomolecule in the presence of the bound water attached at any one of several H-bonding sites on the molecule. Under isolated conditions, when the

laser excitation energy exceeds the dissociation threshold, the flexible product molecule can end up in one of several conformational product wells.¹⁻⁵ In one limit, dissociation could occur on a time scale fast compared to isomerization, thereby favoring a conformational product distribution dominated by the conformational minimum closest to the starting geometry of the complex. In the other extreme, isomerization within the molecule could precede dissociation, leading to a range of conformational products dictated by the potential energy surface for the isomerization within the complex. Furthermore, energy flow in the complex may be such that the exchange between intramolecular and intermolecular modes would lead first to breaking the H bond between water and biomolecule, shuttling the water molecule away from its original site before enough energy flows into the intermo-

^{a)}Author to whom correspondence should be addressed. Electronic mail: zwier@purdue.edu

molecular modes for dissociation to occur. In order to understand these rich dynamics, one would like to determine the conformational product distribution, the rate of dissociation, and the dependence of both these quantities on excess energy, starting geometry, and infrared excited mode.

We have recently introduced the method of stimulated emission pumping–population transfer (SEP-PT) spectroscopy,⁶ and applied it to the study of conformational isomerization in two solute-water complexes of particular relevance to the present work: 3-indole-propionic acid-H₂O (Ref. 7) and *trans*-formanilide-H₂O.⁸ In both cases, the complex is formed under expansion cooling with significant population in more than one conformational minimum. In such a circumstance, SEP-PT can be used to determine the energy barriers to isomerization between these minima.⁶ In the 3-indole propionic acid-H₂O complex, SEP-PT was used to study the effect of complexation of a water molecule on the energy barriers to isomerization of the flexible 3-indole propionic acid molecule.⁷ In the *trans*-formanilide-H₂O complex (TFA-H₂O), the isomerization event involved shuttling the complexed water molecule from one H-bonding site to another on the TFA solute.⁸

In the present work, we study the infrared photodissociation of the tryptamine-H₂O complex, combining aspects of the two previous studies under circumstances where the excitation energy is large enough to dissociate the water molecule from the complex. Tryptamine (3-ethylamine indole) is a prototypical flexible biomolecule that spreads its population over seven conformational minima when it is cooled in a supersonic expansion.^{3,4} The flexibility of the ethylamine side chain in tryptamine (TRA) can be described by two principal flexible coordinates, involving internal rotation about the C(α)-C(β) and C(α)-N single bonds. The three-fold barriers associated with these coordinates lead to nine low-lying conformational minima, of which seven are observed experimentally under supersonic expansion cooling.^{3,5} Interestingly, upon complexation of a single water molecule, the seven conformational isomers of tryptamine collapse to a single structure that retains the same ethylamine side chain conformation present in the most highly populated conformer of tryptamine monomer (conformer A).^{9,10}

Resonant ion-dip infrared spectroscopy was used to determine that the water molecule in TRA-H₂O is bound as a H-bond donor to the nitrogen lone pair of the NH₂ group.¹¹ Recent high resolution UV spectroscopy has confirmed that the water molecule binds at this position, gaining additional stabilization by a second attractive interaction between the C(2)-H of pyrrole and oxygen atom of the water molecule [Fig. 1(a)].¹² The combination of cooling and two-body displacement collisions leads to preferential formation of this “locked-in” structure downstream in the expansion.¹²

Here, we describe measurements of (i) the dissociation energy threshold for the tryptamine-H₂O complex, (ii) the tryptamine monomer product conformational distributions as a function of energy above this threshold, and (iii) the dissociation rates for levels near the threshold, using the techniques of infrared-ultraviolet hole-burning and infrared-ultraviolet hole-filling spectroscopies.¹³ Similar issues of energy flow and the dynamics of dissociation in hydrogen-

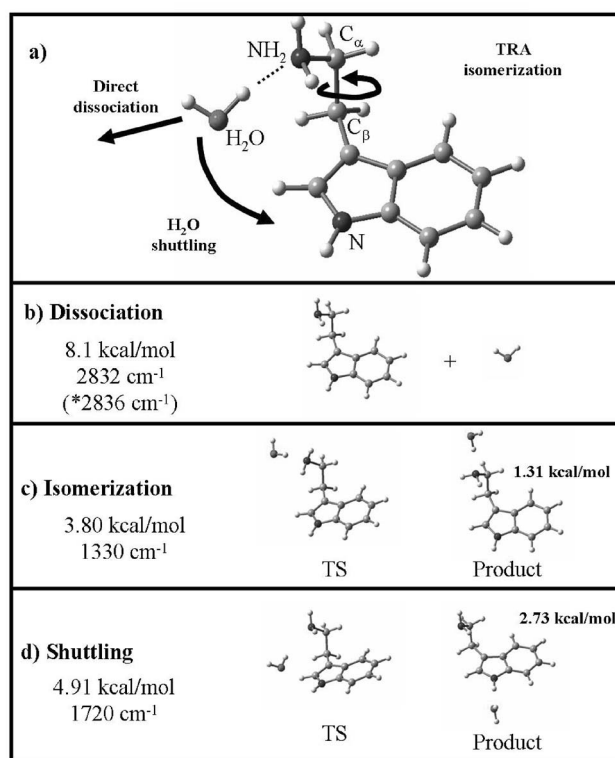


FIG. 1. (a) Schematic diagram of the three competing processes that are energetically feasible following IR photoexcitation of the tryptamine-water complex. The structure shown for the complex is the starting structure for the experiment, known to be the single observed structure for the complex, with an ethylamine side chain conformation close to that of TRA(A) (Refs. 11 and 12). (b)–(d) Calculated structures for the transition states and products of the three competing processes: (b) dissociation, (c) a representative isomerization reaction, and (d) a representative water shuttling reaction. The listed energies, relative to the energy of the initial complex, are from DFT B3LYP/6-31+G* calculations including zero-point energy correction. The number in parentheses in (b) is the final MP2/CBS limit value for the binding energy. See the text for further discussion.

bonded (H-bonded) complexes and other van der Waals complexes have been studied previously,^{14,15} but no studies have probed dissociation in complexes where the products have a significant conformational flexibility, leading to a distribution of conformer products.

Infrared excitation of the tryptamine·H₂O complex was carried out using a series of infrared absorptions spanning the range of 2470–3715 cm⁻¹. A comparison of experimental data to density functional theory computed barriers and *ab initio* binding energies will be made. The rate measurements, carried out under collision-free conditions, beg for comparison with standard statistical theories of the process; most notably, the Rice-Ramsperger-Kassel-Marcus (RRKM) theory.^{16,17} As we shall see, this comparison uncovers a large discrepancy between the two, with the observed rates near threshold orders-of-magnitude faster than the RRKM prediction. Possible reasons for this discrepancy will be discussed.

II. MATERIAL AND METHODS

A detailed description of the instrument and the experimental protocol has been given elsewhere, so that only a brief description is given here.¹⁸ The TRA-H₂O complexes are formed in a supersonic expansion created by a pulsed

valve with a 1.2 mm diameter orifice (General Valve Series 9) operating at 20 Hz to cool the molecules into their conformational zero-point levels (ZPL). Total flow rates of about 100 SCCM (SCCM denotes cubic centimeter per minute at STP) in a 500–750 μ s long gas pulse are typically used. TRA vapor is entrained in 8 bars of helium by heating the solid sample to 140 °C. TRA-H₂O complexes are formed by entraining water vapor at a concentration of 0.03% in the helium mixture. This is accomplished by directing a small portion of the total helium flow over a sample cylinder containing room temperature water vapor via a bypass manifold outfitted with a flow meter and needle valve for flow control.

Hole-filling studies employ a four-step experimental protocol, in which (i) complexes are formed early in the expansion, (ii) selective infrared excitation of the complex occurs following the initial cooling, (iii) the infrared-excited complexes dissociate, and the products are recooled to their zero-point level(s) before (iv) probing the products using LIF with an ultraviolet laser delayed and shifted downstream from the excitation laser. Under typical hole-filling conditions, the infrared output of an infrared parametric converter (LaserVision) crosses the expansion 2.5 nozzle diameters downstream from the expansion orifice (i.e., $x/D=2.5$, where x is the distance between the nozzle orifice and the excitation point and D is the nozzle diameter), while the UV probe laser (doubled, neodymium-doped yttrium aluminum garnet-pumped dye laser) intersects the expansion at $x/D\sim 7$. A delay of ~ 2 μ s separates the two laser pulses, a time sufficient for the IR-excited molecules to traverse the distance between the two laser beams. Based on laser-induced fluorescence spectra recorded at $x/D=2.5$, hot band intensities were used to estimate a vibrational temperature of about 10–15 K at the point of infrared excitation. Infrared pulse energies are typically chosen so as to induce significant fractional population depletion on the strong infrared spectral bands in the absence of recoiling collisions (30%–50% depletion).

In order to detect only the changes induced by the infrared laser, the change in fluorescence signal induced by the infrared laser was recorded using active base line subtraction of the signal via an in-house LABVIEW programming environment. The infrared laser (10 Hz) is pulsed every other time the UV laser fires (20 Hz). A negative (positive) signal indicates a depletion (gain) in the fluorescence signal.

The primary interest of the present study is to determine the product distribution of the TRA conformers formed in the IR photodissociation. IR-UV hole-filling spectroscopy is well suited for that purpose. The infrared laser is held fixed at a wavelength where selective infrared excitation of a single conformation can be carried out. The ultraviolet laser is then tuned through the transitions of interest in the laser-induced fluorescence (LIF) spectrum. Dips in population will be seen as depletions in the LIF spectrum, while gains in population will produce positive-going signals. A general strength of hole-filling methods when applied to conformational isomerization is that it utilizes conformation-selective excitation and detection steps, thereby providing a means of dissecting the complicated set of isomerization processes into individual $X\rightarrow Y$ reactant-product pairs. In the present

context of infrared photodissociation, the single starting geometry for the TRA-H₂O complex is known,^{10,19} but many TRA monomer conformations can be formed as products. As a result, IR-UV hole-filling spectroscopy can be used to determine where the population went following infrared excitation of a single conformer.

The IR-UV hole-filling scheme just described uses the recoiling collisions in order to determine the conformational product distributions formed. As we shall see, the recoiling step is needed because without it, excess internal energy in the TRA monomer products quickly broadens the UV spectra of the products to the point that conformational identification is quickly lost. However, right near the dissociation threshold, it is possible to probe the dissociation rate and product distribution in the absence of collisions. In that case, the IR is brought downstream to overlap with the UV probe laser (typically at $x/D\sim 25$). The method is then called IR-UV hole-burning spectroscopy.²⁰

Tryptamine was used as received (Aldrich), whereas deuterated tryptamine was formed by isotopic exchange in D₂O solution containing DCl (35 wt %) and by stirring for 30 minutes, followed by precipitation with NaOD (40 wt %), and washing with D₂O. The sample was dried and stored under nitrogen. Back exchange was prevented by keeping a steady flow of D₂O over the sample throughout these experiments.

TRA has three exchangeable hydrogens: the two amino hydrogens and the indole NH, with the former more easily exchanged than the latter. Despite repeated exchange cycles, complete deuteration at all three sites was never achieved, probably due to back exchange in the sample compartment. The degree of isotopic substitution was assessed using resonant two-photon ionization (R2PI) spectroscopy. Based on intensities of the origin transitions, it was determined that more than 90% of the sample was either doubly or triply deuterated, with nearly complete deuteration at the ND₂ site anticipated.

III. CALCULATIONS

A. Starting geometry, transition states, and vibrational analysis

The global minimum geometry computed for the TRA-water complex is consistent with that obtained experimentally,^{10,12,19} with water acting as a H-bond donor to the amino group of the ethylamine side chain [Fig. 1(a)]. This structure serves as the starting geometry for the infrared photodissociation process. In the complex, the ethylamine side chain adopts a Gpy(out) configuration similar to that of TRA(A), the known global minimum on the TRA monomer surface.^{5,12} In so doing, the water molecule can receive additional stabilization from a pyrrole CH \cdots O interaction.

As a first step in understanding the competing processes involved, optimized transition states for dissociation out of the TRA(A)-H₂O well and isomerization to TRA(B)-H₂O, and for shuttling the water molecule between the amino and indole NH sites were calculated using density functional theory (DFT) at the 6-31+G* level²¹ with the Becke3-Lee-Yang-Parr (B3LYP) functional.²² The GAUSSIAN 03 (G03) pro-

gram suite was used for these calculations, with ultrafine grids and the tightest convergence criteria available in G03 employed in the optimization. Zero-point corrections to the energies were calculated using harmonic vibrational frequencies.²³ The geometries and energies of the transition states are depicted in Figs. 1(b)–1(d).

The conformational isomerization from TRA(A)-H₂O to TRA(B)-H₂O was predicted to have a zero-point corrected transition state 1330 cm⁻¹ (3.80 kcal/mol) above the global minimum TRA(A)-H₂O structure, whereas the corresponding value for the water shuttling reaction between the amino and indole NH groups is about 1720 cm⁻¹ (5 kcal/mol) including zero-point correction. These transition states were located using quadratic linear searches with optimized transition state structures²⁴ verified by the presence of a single imaginary frequency along the “reaction” coordinate in the harmonic normal modes. Both of these barriers are well below the predicted binding energy (next section), indicating that the isomerization and shuttling reactions can occur in the water complex at energies well below the dissociation threshold.

The binding energy of the complex was also computed at this level of theory [Fig. 1(b)]. However, because a highly reliable value for the binding energy is important to a comparison with our experimental data, calculations employing higher levels of theory were also undertaken, which will be described in Sec. III B.

One of the intriguing aspects of the study of the photodissociation of TRA-H₂O is the contrast it gives with similar studies on smaller water-containing clusters which lack the flexibility of the TRA “solute.” In general, complexation of a single water molecule to a polyatomic solute produces a set of six intermolecular vibrations that asymptotically correlate with the three translational and three rotational degrees of freedom of the free water monomer. The vibrational frequencies of these intermolecular degrees of freedom are typically rather low in frequency, covering a range of tens to hundreds of wave numbers. In small complexes such as the water dimer, the intramolecular vibrational frequencies of the water monomer are much higher in energy, and are thus well separated from the intermolecular modes, as shown in Fig. 2. This clear energy separation leads to a bottleneck in energy flow between the intramolecular and intermolecular modes in small molecule-H₂O complexes. On the other hand, in TRA-H₂O, this gap is closed because the TRA monomer itself already possesses many low frequency modes that intermingle with the intermolecular modes, as shown schematically in Fig. 2. As a result, energy flow is anticipated to be facile between the ethylamine torsional and intermolecular degrees of freedom.

B. Binding energy calculations

DFT is used widely to compute the structures and vibrational frequencies of complexes due to its reasonable accuracy and comparative speed. However, because it does not properly account for dispersion forces, DFT calculations of the binding energy of complexes fall under close scrutiny.²⁵ In certain circumstances, the results are surprisingly good.

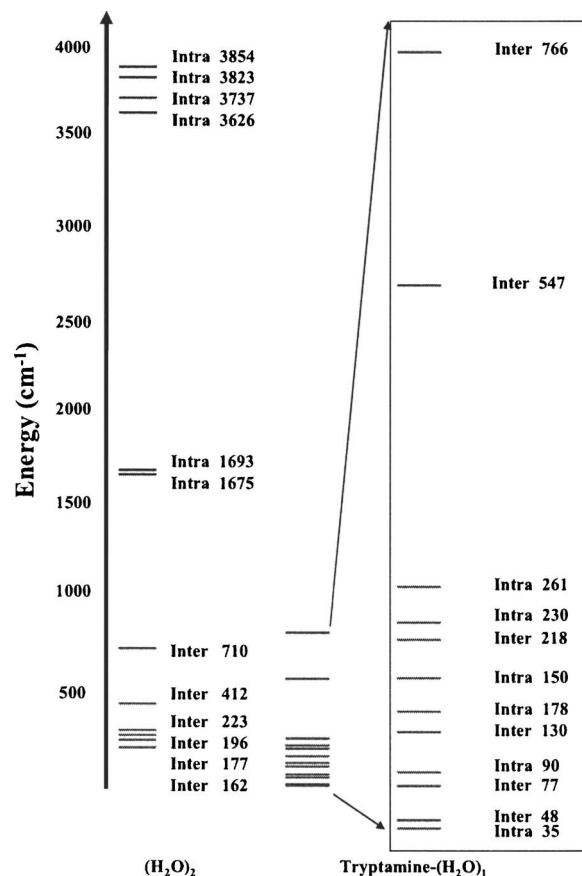


FIG. 2. A comparison of harmonic vibrational frequencies (in cm⁻¹) of the water dimer to the six lowest inter- and six lowest intramolecular modes of the tryptamine-water complex at the B3LYP/6-31+G* level of theory. Note that the two types of modes are intermingled with one another in the TRA-H₂O complex.

For instance, when applied to strongly H-bonded complexes, DFT does account for a substantial fraction of the dispersion interactions due to a significant overlap of electron densities from the two fragments.²⁵

As a starting point for our discussion, then, Table I presents the calculated binding energy of TRA-H₂O and TRA(*d*₃)-D₂O at the DFT B3LYP/6-31+G* level of theory. The binding energy predicted in this way is 2632 cm⁻¹ for TRA-H₂O and 2825 cm⁻¹ for TRA(*d*₃)-D₂O, consistent with the observed lower and upper bounds on the threshold for TRA(*d*₃)-D₂O (2745 and 2869 cm⁻¹, respectively). We also estimated the basis set superposition error (BSSE) correction via counterpoise correction²⁶ (Table I).

The interpretation of our experimental data for TRA-H₂O depends very critically on the magnitude of the binding energy. In DFT calculations, the close correspondence between calculated binding energies and experiment may result from a fortuitous cancellation of errors associated with an improper description of dispersion forces coupled with an overestimate in the counterpoise correction.²⁷ As a result, we have made an attempt to estimate the binding energy at the highest levels of *ab initio* theory currently feasible for a complex of this size. As described in detail below, the TRA-H₂O geometry was optimized at either the second-order Moller-Plesset (MP2) or the (RIMP2) level, using several different basis sets. At each of these geometries, a series

TABLE I. Calculated binding energies (zero-point energy corrected with and without counterpoise correction) at various levels of theory, compared to experimental bounds.

	Level of theory	D_0 (kcal/mol)	D_0 (cm ⁻¹)	D_0 (kcal/mol) (counterpoise)	D_0 (cm ⁻¹) (counterpoise)
TRA-Water	B3LYP/6-31+G ^{*a}	7.52	2632	6.41	2243
	RIMP2/CBS ^b	7.39	2587	7.53	2636
TRA-D ₂ O	B3LYP/6-31+G ^{*a}	8.06	2821	6.77	2371
	RIMP2/CBS ^b	7.93	2776	8.07	2825
	Expt.	7.84–8.20	2745–2872	7.84–8.20	2745–2872

^aUsing B3LYP/6-31+G^{*} Harmonic ZPE frequencies (protonated=2.48, and deuterated=1.94).

^bResolution of identity MP2 with complete basis set extrapolation. We take this value to be the most accurate.

of RIMP2/aug-cc-pVXZ ($X=D, T, Q$) single-point calculations was performed, from which the binding energy was extrapolated to the complete basis set limit. Here, “RIMP2” denotes the resolution-of-identity (RI) approximation^{28,29} to the canonical MP2 theory. This method greatly reduces the cost of MP2 calculations by introducing an auxiliary basis set to eliminate four-index integrals and has been shown to introduce negligible errors in MP2 energy differences when optimized auxiliary basis sets are used.^{29,30} Our calculations utilize the auxiliary basis sets of Weigend *et al.*,³¹ which are optimized for use with standard correlation-consistent aug-cc-pVXZ basis sets. All MP2 and RIMP2 calculations in this work use frozen core orbitals and were performed using Q-CHEM v.3.0,³² which includes an efficient implementation of the RIMP2 analytic gradient.³³

Complete basis set (CBS) estimates of the RIMP2 binding energy were obtained by separate extrapolation of the absolute energies of the monomers and the complex. Hartree-Fock energies were extrapolated via a three-point exponential ansatz, $E_{\text{HF}}(X) = E_{\text{HF}}(\infty) + ae^{-\beta X}$ (where $X=2, 3$, and 4 for D, T, and Q, respectively), while correlation energies were extrapolated using a two-point linear extrapolation, excluding the RIMP2/aug-cc-pVDZ data point. This procedure has been recommended on the basis of benchmark calculations in very large basis sets.³⁴

The RIMP2 binding energies are listed in Table II, both with and without counterpoise correction.²⁶ As expected, the uncorrected (and therefore BSSE-contaminated) binding energies approach the CBS limit from above, while the counterpoise-corrected binding energies approach the CBS limit from below. Following extrapolation, there is good agreement between the corrected and uncorrected binding energies, as BSSE should approach zero in the CBS limit.

An important conclusion that emerges from these RIMP2 calculations is that the computed binding energy varies significantly based on whether or not diffuse basis functions are included in the geometry optimization. Following Schmitt *et al.*,³⁵ we initially optimized geometries at the MP2/6-311G^{**} level. At this geometry, the RIMP2/CBS estimates of D_e are 9.04 and 9.12 kcal/mol with and without counterpoise correction, respectively. Using MP2/6-311G^{**} harmonic frequencies, we obtain a zero-point correction of -3.31 kcal/mol and thus a D_0 of 5.73–5.81 kcal/mol, far below the experimental value. (For comparison, Schmitt

*et al.*³⁵ obtained $D_0=4.8$ kcal/mol at the same geometry, using DFT frequencies to correct the MP2/6-311G^{**} estimate of D_e .)

The primary source of this discrepancy turns out to be the basis set that is used to optimize the geometry. BSSE contaminates not only the single-point energies but also the energy gradients used in geometry optimization, but inclusion of diffuse basis functions (which serve to reduce BSSE) in the geometry optimization can often mimic the effects of using a proper (but very expensive) counterpoise-corrected energy gradient.³⁶ With this in mind, we reoptimized the geometries of the complex and the monomers using several different basis sets that include diffuse functions (see Table II). This has a dramatic effect, increasing the RIMP2/CBS binding energy by 0.8–1.2 kcal/mol relative to the value at the MP2/6-311G^{**} geometry. Adding a second set of diffuse functions [MP2/6-311(2+, 2+)G^{**} optimization] changes the binding energy by less than 0.05 kcal/mol.

For optimization of the geometry, we are unable to probe the basis set limit directly because optimization at the RIMP2/aug-cc-pVTZ level is prohibitively expensive. However, the change from a double- ζ to a triple- ζ basis appears to matter far less than the inclusion of diffuse basis functions. For example, MP2/6-31+G^{*} geometries yield binding energies within 0.2–0.3 kcal/mol of those obtained at the

TABLE II. RIMP2/aug-cc-pVXZ and RIMP2/CBS binding energies (not including zero-point energy correction) for the tryptamine-H₂O complex.

Geometry	X	Counterpoise-corrected ^a	Uncorrected ^a
MP2/6-311G ^{**}	D	8.08 (8.19)	10.22 (10.33)
	T	8.68 (8.95)	9.73 (10.00)
	Q	8.89 (9.25)	9.35 (9.71)
	CBS	9.04 (9.45)	9.12 (9.53)
MP2/6-311+G ^{**}	D	9.05 (9.08)	11.15 (11.18)
	T	9.52 (9.87)	10.53 (10.88)
	Q	10.46 (10.86)	10.12 (10.52)
	CBS	10.66 (10.70)	10.27 (10.31)
RIMP2/aug-cc-pVDZ	D	8.85 (9.30)	10.96 (11.41)
	T	9.42 (10.05)	10.44 (11.07)
	Q	9.60 (10.33)	10.08 (10.81)
	CBS	9.75 (10.54)	9.89 (10.68)

^aAdiabatic binding energies, with the vertical binding energies in parentheses.

MP2/6-311++G** (or the RIMP2/aug-cc-pVDZ) geometry, whereas MP2/6-31G* geometries afford binding energies close to those obtained at the MP2/6-311G** level. Therefore, we do not expect that optimization at the RIMP2/aug-cc-pVTZ level would have a large effect on the binding energy.

Correlation-consistent basis sets are preferable for the computation of *ab initio* vibrational frequencies,³⁷ and we regard the RIMP2/aug-cc-pVDZ geometry as the most reliable. Using RIMP2/aug-cc-pVDZ harmonic frequencies, we obtain a zero-point energy correction of -2.29 kcal/mol, significantly smaller than the zero-point correction at the MP2/6-311G** level. Additional calculations reveal that the zero-point correction is consistently reduced by about 1.0 kcal/mol whenever diffuse functions are included in the geometry and frequency calculation. (For example, the zero-point correction at the MP2/6-31+G* level is -2.58 kcal/mol.) Based on these observations, we put forward our RIMP2/CBS||RIMP2/aug-cc-pVDZ calculation as the most accurate existing theoretical estimate of the tryptamine-H₂O binding energy. The RIMP2/CBS counterpoise-corrected binding energy is 9.75 kcal/mol (9.89 kcal/mol without counterpoise correction); combining this with the aforementioned zero-point correction, we obtain an estimated adiabatic binding energy of 7.46 kcal/mol (2609 cm⁻¹) with counterpoise correction and of 7.60 kcal/mol (2658 cm⁻¹) prior to counterpoise correction.

In order to extrapolate this calculated value to the corresponding value in TRA(*d*₃)-D₂O, the zero-point energy (ZPE) correction was recalculated for this isotopomer, leading to an increase in binding energy of 189 cm⁻¹. As a result, the calculated “best value” for $D_0(\text{TRA}(d_3)\text{-D}_2\text{O}) = 8.07$ kcal/mol (2825 cm⁻¹). Much of this difference is due to changes in the frequencies of the O–D stretch and the intermolecular vibrations of the complex.

The comparison with experiment is left until the measurements have been described in the following section. This state-of-the-art binding energy calculation can be directly compared with the experimental thresholds in order to assess whether the observed dissociation thresholds are affected significantly by a kinetic shift.

IV. EXPERIMENTAL RESULTS

A. LIF

As a starting point for our dynamical studies, we have recorded LIF excitation spectra of TRA monomer and TRA-H₂O. These are similar to those already reported by our group^{4,5} and others.^{1,3,9,10,12,38} The LIF and R2PI spectra of TRA(*d*₃) and TRA(*d*_{*n*})-D₂O have also been studied previously.^{2,12,39} We have used R2PI spectroscopy to identify transitions associated with different numbers of deuterium substitutions. For our purposes, these data were used to identify the carrier of transitions in the LIF spectrum, thereby confirming that the amino and indole NH groups were deuterated under the conditions of the hole-filling study of TRA(*d*_{*n*})-D₂O. Only the S_0 - S_1 origin transitions of the isotopomers were of relevance to the present work, serving as monitor transitions for the hole-filling studies.

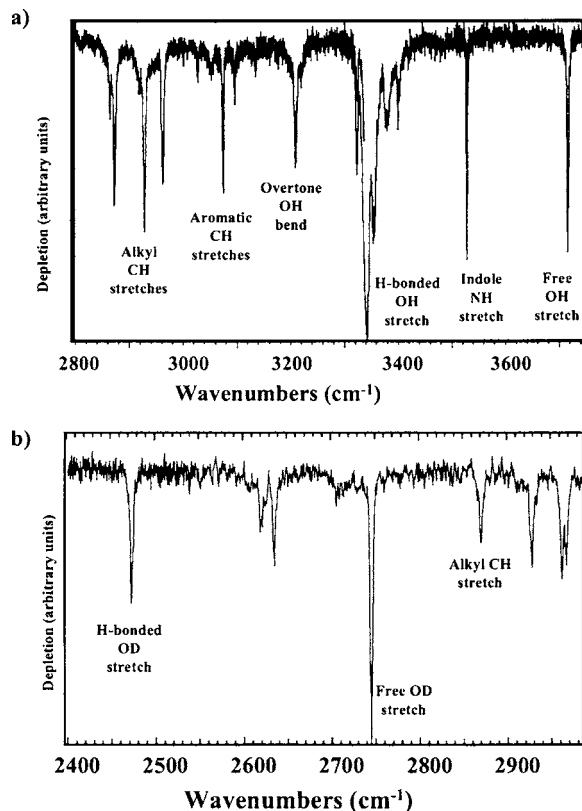


FIG. 3. (a) FDIR spectrum of the tryptamine-water complex in the hydride stretch region of the infrared (2800–3750 cm⁻¹). The free OH (OD) stretch, H-bonded OH (OD) stretch, the overtone of the OH bend, and the lowest frequency alkyl CH stretch (2872 cm⁻¹) were used for selective photodissociation of the TRA-H₂O complex. (b) FDIR spectrum of the tryptamine(*d*₃)-D₂O complex taken over the 2400–3000 cm⁻¹ region. The free OD stretch, H-bonded OD stretch, and the lowest frequency alkyl CH stretch (2869 cm⁻¹) were used for selective photoexcitation of the TRA(*d*₃)-D₂O complex.

B. Fluorescence-dip infrared spectra

Figures 3(a) and 3(b) present the fluorescence-dip infrared (FDIR) spectra in the hydride stretch region of both TRA-H₂O and TRA(*d*₃)-D₂O. The spectrum of TRA-H₂O [Fig. 3(a)] is essentially identical to that published earlier by our group, which provided clear evidence that the H₂O molecule was bound on the amino site of TRA via a single, strong H bond.¹¹ This complexation produces a free OH stretch (3716 cm⁻¹) due to the unbound water OH group, a H-bonded OH stretch fundamental, with its large intensity and broadening (~ 3340 cm⁻¹), and an overtone of the OH bend (3208 cm⁻¹). The assignments of the other IR transitions are also summarized in Fig. 3. The symmetric CH stretch at 2872 cm⁻¹ exhibits a small satellite band about 9 cm⁻¹ to the red spectrum which can be attributed to a Fermi resonance with a CH bend overtone.

All of the labeled transitions in the IR spectra of Fig. 3 are unique to the TRA-H₂O or TRA(*d*_{*n*})-D₂O complexes. This uniqueness is true even for the 2872/2869 cm⁻¹ alkyl CH stretch fundamentals, which are shifted away from any of the observed transitions due to the various conformers of TRA monomer.⁵ As a result, these transitions can serve as a means of selective IR excitation of the complex in order to initiate IR photodissociation of the complex. Selective exci-

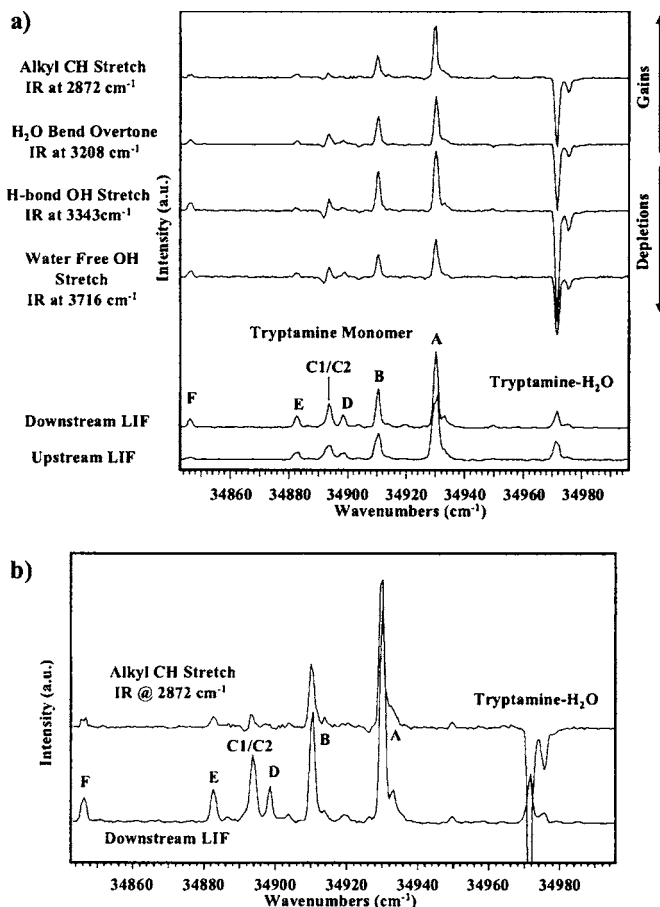


FIG. 4. (a) Top four traces: IR-UV hole-filling spectra with the IR photoexcitation frequency fixed at the indicated wave number position at the peak of the indicated absorption of TRA-H₂O. The depletion in the TRA-H₂O transitions leads to gains in the populations of the TRA monomer products following dissociation of the complex. Bottom two traces: Downstream and upstream LIF are excitation spectra taken at the probe and pump excitation points, respectively. The similar ratio of TRA-H₂O to TRA monomer signal indicates that complex formation is complete at the point in the expansion where IR excitation occurs. (b) Expanded view of IR-UV HF scan when pumping the alkyl CH stretch at 2872 cm⁻¹, compared to the downstream LIF scan. Note that the product yield shows a distinct preference for TRA(A, B) relative to the populations in the absence of IR excitation.

tation of a well defined hydride oscillator of TRA-H₂O will give the complex energies ranging from 2872 to 3715 cm⁻¹, depending on the excited mode. Upon deuteration, the free and H-bonded OD stretch fundamentals shift to 2745 and 2470 cm⁻¹, respectively [Fig. 3(b)].

C. Hole-filling spectroscopy

IR-UV hole-filling spectroscopy was used to study the product TRA monomer conformational product distribution following selective IR excitation of the TRA-H₂O or TRA(*d*₃)-D₂O complexes. By carrying out the selective IR excitation of the TRA-H₂O or TRA(*d*₃)-D₂O complexes early in the expansion, the dissociated monomer products could be recooled to their zero-point levels prior to LIF detection. Four IR-UV hole-filling spectra recorded with IR excitation at 2872, 3208, 3343, and 3715 cm⁻¹ are shown as the top four traces in Fig. 4(a). They are compared to LIF excitation spectra recorded with the probe laser downstream in the collision-free region of the expansion (its normal po-

sition in a hole-filling experiment) or upstream with the probe laser translated upstream to the point where IR excitation occurs in the collisional region of the expansion. A comparison of the intensities of the TRA-H₂O and TRA monomer transitions in the upstream and downstream LIF scans indicates that TRA-H₂O complex formation is complete at the point of IR excitation. As a result, we do not have to be concerned with the formation of TRA-H₂O complexes after the point of IR excitation, which could muddle the interpretation of the hole-filling results. Furthermore, while the width of the rotational band contours is larger in the upstream LIF scan, there is no evidence of hot bands of TRA-H₂O, so that IR excitation of the complex occurs only from the ZPL of the complex.

The hole-filling scans in Fig. 4(a) are difference spectra that compare the LIF signal from the probe laser with the IR present to that without the IR. As a result, negative-going peaks indicate a depletion in population of the species responsible for that transition, while positive-going signals arise from an increase in population. As anticipated, the chosen IR wave number positions cause a selective excitation of the TRA-H₂O complex, thereby partially depleting its ground state population and leading to a negative-going peak at its position in the LIF scan. The loss of population in the complex is accompanied by corresponding gains in the population of TRA monomer conformations due to the fragmentation of the complex and recoiling of the TRA monomer product into the various conformational zero-point levels. The small depletion signal at 34 890 cm⁻¹ is due to a weak transition associated with the TRA-(H₂O)₂ cluster, which also absorbs at the IR wavelengths used for the scans. The population of this cluster is small compared to the TRA-H₂O complex under the low H₂O flows used for these scans. At all four excitation energies, dissociation occurs during the 2 μs delay between pump and probe lasers.

In all four hole-filling scans of Fig. 4(a), the TRA monomer conformational product distribution is dominated by population gains in conformers A and B; that is, Gpy(out) and Gpy(up). Small amounts of the other conformers are also observed, with slightly greater intensities at higher energy. Figure 4(b) shows a close-up view comparing the hole-filling scan at 2872 cm⁻¹ with the downstream LIF spectrum. This comparison highlights the dominance of conformers A and B in the hole-filling scan, where transitions due to conformers C–F are hardly visible compared to their intensities in the LIF scan below it.

Perhaps the most obvious deduction from the IR-UV hole-filling spectra of Fig. 4 is that dissociation is energetically feasible at all infrared energies between 2872 and 3715 cm⁻¹. As a result, in order to locate the dissociation threshold, analogous scans were taken on the TRA(*d*₃)-D₂O complex, which possesses OD stretch transitions at still lower energies [2745 and 2470 cm⁻¹, Fig. 3(b)]. Figure 5 presents IR-UV hole-filling scans recorded at 2745 cm⁻¹ (upper trace) and at 2869 cm⁻¹ (lower trace). Clear gains are observed at 2869 cm⁻¹ excitation energy, but no gains are observed at 2745 cm⁻¹, despite the fact that the latter transition is several times more intense than the alkyl CH stretch transition at 2869 cm⁻¹. A much smaller dip signal is ob-

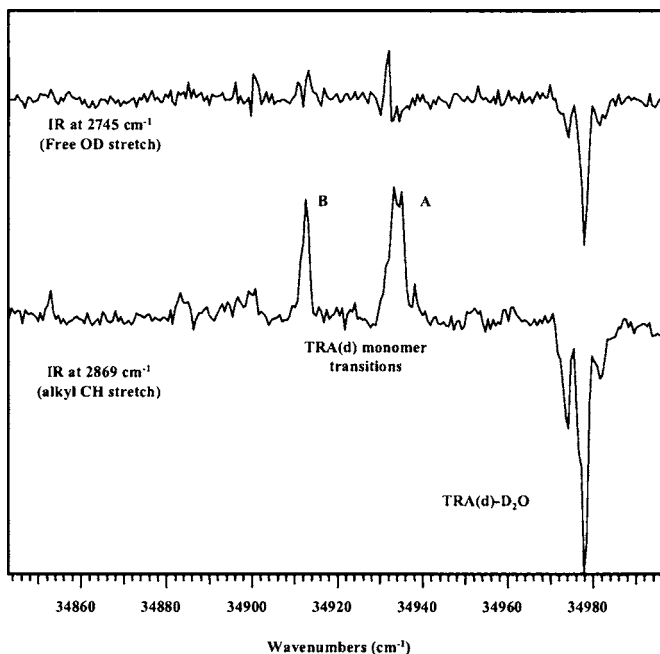


FIG. 5. The IR-UV HF spectrum exciting the 2745 cm^{-1} (upper trace) and the 2869 cm^{-1} (lower trace) bands of $\text{TRA}(d_3)\text{-D}_2\text{O}$ while tuning the probe laser. No dissociation is observed in the upper trace, while dissociation product signals due to conformers A and B of TRA monomer are clearly observed in the lower trace and dominate the products formed. The lack of gain signal in the upper trace indicates that no dissociation occurs on the time scale of the experiment ($\sim 2\ \mu\text{s}$) at that excitation energy.

served at 2745 cm^{-1} , indicating that recoiling the undissociated complex is not complete at the downstream probe position. This remaining dip is consistent with the fact that recoiling must remove the full 2745 cm^{-1} if it is below threshold, while the dip at 2869 cm^{-1} is larger because some of the complex has dissociated. As an additional check, no gain is observed following excitation of the even stronger IR transition due to the H-bonded OD stretch at 2470 cm^{-1} (not shown). In conclusion, the hole-filling data have placed a clear upper bound to the binding energy of the complex at 2869 cm^{-1} . The absence of monomer gains at 2745 cm^{-1} is a likely indicator that this transition is below the dissociation threshold. However, the absence monomer signal at 2745 cm^{-1} could also result if the time scale for dissociation were too slow to be observed in the $2\ \mu\text{s}$ time window between excitation and probe.

D. IR-UV holeburning

One of the ways in which one can confirm that the observed energy threshold for dissociation is, in fact, a measure of the binding energy for the complex (rather than a threshold determined by a kinetic shift) is to probe the TRA monomer products under collision-free conditions. If the infrared transition at which products are first observed is very close to the true binding energy, then the vast majority of the energy gained by absorption of an infrared photon will be used up in breaking the $\text{TRA-H}_2\text{O}$ bond, leaving very little internal energy in the TRA monomer. In order to check this point, we carried out IR-UV hole-burning scans as a function of energy above threshold. These are presented in Fig. 6(a). As anti-

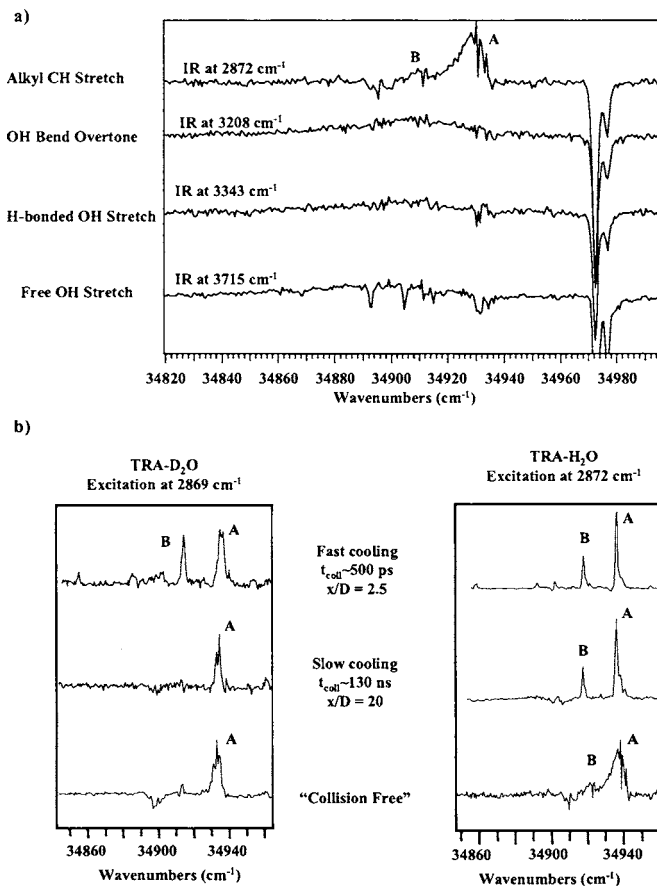


FIG. 6. (a) Collision-free IR-UV hole-burning spectra following excitation at 2872 , 3208 , 3343 , and 3715 cm^{-1} (the same excitation energies as in Fig. 3(a)). In the absence of cooling collisions, the TRA monomer product signals are broadened due to the internal energy present in the TRA monomer products. At 2872 cm^{-1} excitation energy, distinct signals due to TRA(A, B) are still resolvable. (b) IR-UV spectra of $\text{TRA-H}_2\text{O}$ and $\text{TRA}(d_3)\text{-D}_2\text{O}$ are compared following infrared excitation at the indicated position in the supersonic expansion (x is the distance from the nozzle orifice and D is the nozzle diameter). t_{coll} = the calculated time between collisions at that excitation position. See text for further discussion.

ated, at 2872 cm^{-1} excitation energy, the first transition where TRA monomer products are observed under hole-filling conditions, the TRA monomer bands observed in the absence of collision are narrow enough ($\sim 15\text{ cm}^{-1}$ full width at half maximum) to distinguish the main band as due to TRA(A). Note that in the absence of collisions at threshold, TRA(A) dominates the products, with a small amount of B present as a weak shoulder, as labeled in the upper trace.

As the internal energy is raised above this threshold (lower three traces), conformation-specific information is quickly lost as the TRA monomer bands broaden to the point that they cannot be distinguished from one another. These scans show clearly why it is necessary to recool the products using hole-filling conditions if one is to determine conformation-specific product yields.

The increasing breadth at higher excess energy reflects the fact that much of the excess energy is going into internal energy in the TRA monomer products. In principle, any excess energy could be distributed between product translation and the rotational and vibrational degrees of freedom of the TRA and water monomer products. However, of these, the

only significant sink for internal energy is the TRA monomer vibrations because these are low enough in frequency to be populated near threshold. Rotational excitation in the product is restricted by angular momentum conservation. Furthermore, previous studies of the product state distributions following photodissociation of van der Waals complexes have detected only small amounts of energy appearing in translation.⁴⁰

Figure 6(b) compares the product distribution for TRA(*d*₃)-D₂O to that for TRA-H₂O at threshold (2869 or 2872 cm⁻¹ excitation energy) under collision-free, slow-cooling, and fast-cooling conditions. The position of the IR laser excitation (in nozzle diameters, *x/D*) is listed on each trace, along with a calculated time between collisions with helium at that point in the expansion.^{41,42} The set of scans due to TRA-H₂O shows a product distribution composed exclusively of TRA(A) and TRA(B), with little change in the relative integrated intensities of the products with cooling rate. The TRA(*d*₃)-D₂O scans are more intriguing. First, under collision-free and slow-cooling conditions, only TRA(A) is observed, consistent with the increased binding energy of the TRA(*d*₃)-D₂O (Table I) relative to TRA-H₂O, which may energetically close off the formation of the higher energy TRA(B) conformer.³⁹ Second, under fast-cooling conditions, both TRA(A) and TRA(B) are formed. Possible reasons for this change in product distribution will be discussed further in Sec. V.

E. Dissociation rates

The threshold studies described in the last section demonstrated conformation-specific detection even under collision-free conditions. Furthermore, despite the fact that conformation specificity is lost at higher energies, it should be possible to directly measure the rate of dissociation of the complex as a function of internal energy under collision-free conditions. To that end, Fig. 7 presents a series of scans in which the time delay between the IR excitation and UV probe laser was scanned while monitoring either the disappearance of the TRA-water complex or the appearance of the TRA monomer product. These timing scans were carried out in the “collision-free” region of the expansion (*x/D*=30) where collisions are estimated to occur slower than 200 ns.

Figure 7 presents a set of six time-delay scans, in three sets of two, associated with infrared excitation of TRA-H₂O at 3208 cm⁻¹ (top) and 2872 cm⁻¹ (middle), and of TRA(*d*₃)-D₂O at 2869 cm⁻¹ (bottom). These scans are recorded in the active base line subtraction mode in which the IR laser is pulsed at 10 Hz, and the UV probe laser at 20 Hz, thereby recording the change in population induced by the IR laser. The three depletion scans are recorded by monitoring the *S*₀-*S*₁ origin transition of the TRA-H₂O or TRA(*d*₃)-D₂O reactant, while the gain spectra result when monitoring the peak of the monomer signal at that IR excitation energy [see Fig. 7(a)]. In the reactant depletion traces, the initial depletion reflects the decrease in cold water complex signal due to absorption of the infrared photon. The resulting UV spectra of the “hot” complexes are very broad, even before dissociation occurs, and are reflected in an onset for the depletion

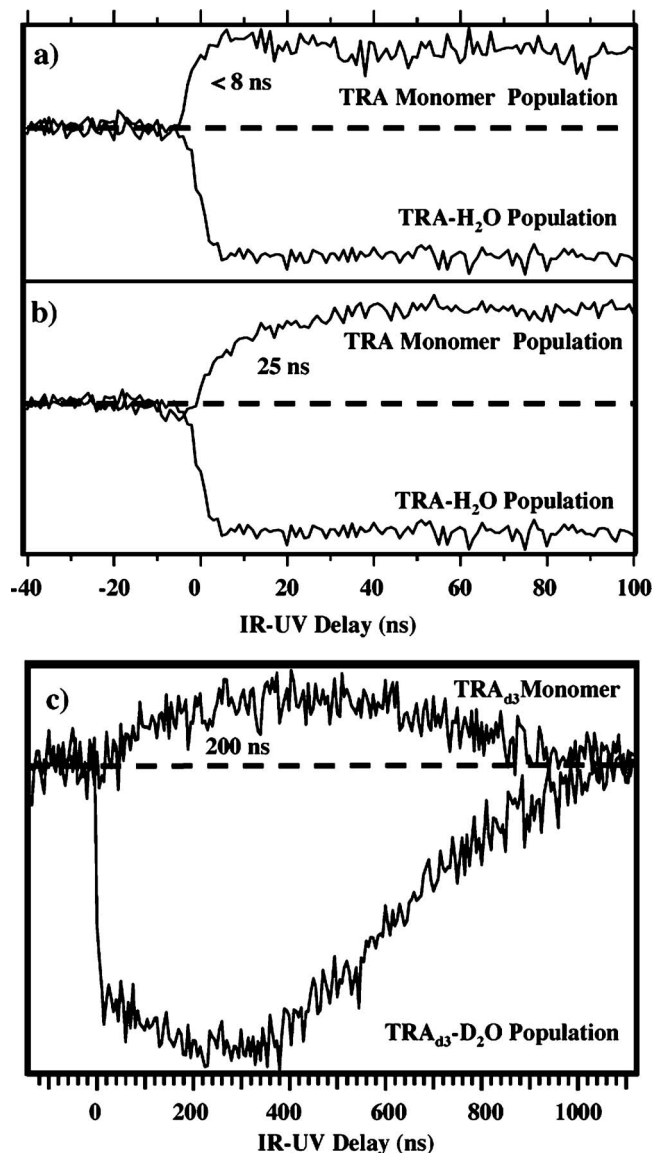


FIG. 7. [(a)–(c)] Timing scans taken under collision-free conditions with the IR and UV laser beams overlapped while scanning the time delay between the two lasers. The lower trace in each set is a depletion scan recorded with the UV laser fixed at the peak of the cold [(a) and (b)] TRA-H₂O *S*₀-*S*₁ origin transition or (c) TRA(*d*₃)-D₂O, while the upper traces were recorded with the UV laser fixed at the *S*₀-*S*₁ origin of [(a) and (b)] TRA(A) or (c) TRA(A,*d*₃). The IR is fixed at (a) 3208 cm⁻¹ and (b) 2872 cm⁻¹ in TRA-H₂O or at (c) 2869 cm⁻¹ in TRA(*d*₃)-D₂O. The sharp onset in the depletion scans reflects the formation of “hot” TRA-water complexes following IR absorption. The time dependence of the monomer gain signal reflects the time-dependent dissociation of the complex. Note the different time scales on (a) and (b) relative to (c). See the text for further discussion.

which is laser pulse limited. By comparison, the onset of the gain signal due to the monitor shows a slower rise due to dissociation of the complex. At long times in all traces, the difference signal returns back to zero due to the fact that the species absorbing the infrared radiation move downstream with time, out of the spatial region probed by the UV probe laser. The monomer temporal profiles are fit to a sum of a rising and falling exponentials (due to dissociation and overlap, respectively) to obtain the dissociation lifetime. These are also listed in Table IV.

It is especially striking that excitation at the correspond-

ing alkyl CH stretch fundamental of TRA-H₂O (2872 cm⁻¹) and TRA(*d*₃)-D₂O (2869 cm⁻¹) yield dissociation rates differing by an order of magnitude. This large difference between the deuterated and protonated complexes is due, at least in part, to a zero-point effect that increases the binding energy of the TRA(*d*₃)-D₂O complex relative to that for TRA-H₂O. As Table I indicates, the calculated increase in binding energy is approximately 189 cm⁻¹, independent of whether harmonic or scaled frequencies are used. As a result, near threshold, this difference in binding energy will lead to large changes in the dissociation lifetime, as the number of product vibrational levels available to the complex increases quickly with excess energy.

The analogous scan following excitation of TRA-H₂O at 3208 cm⁻¹ has a rise time limited by the laser pulse (8 ns), consistent with the expected fast increase in the density of product states with increasing energy above threshold.

The data contained in Figs. 5–7 provide unequivocal evidence for a dissociation threshold for TRA-H₂O at 2872 cm⁻¹ and for TRA(*d*₃)-D₂O at 2869 cm⁻¹, with the latter excitation energy closer to the binding energy than the former. Furthermore, the narrow width of the monomer transitions is indicative of small excess internal energy in the TRA monomer products, consistent with this threshold being near the true binding energy. In addition, the lack of any measurable gain due to TRA monomer at 2745 cm⁻¹ enables us to place an upper bound on the dissociation lifetime at that energy of ~5 μs. As stated earlier, the most plausible reason for the lack of signal is that 2745 cm⁻¹ is below the binding energy of TRA(*d*₃)-D₂O; however, we will consider this and other options more thoroughly in the following section.

V. DISCUSSION

The experimental results on the infrared photodissociation of TRA-H₂O have raised several important issues to which we return to address in this section more fully. First, it is necessary to consider the body of evidence regarding the experimental bounds on the binding energy of the complex since its magnitude is crucial to our assessment of the product yields and dissociation rates. Second, we will consider further the unusual threshold collisional effects on the observed TRA product conformational distribution. This will provide insight to the competition between dissociation, isomerization, and water shuttling. Finally, the experimental dissociation rates near threshold will be compared to the predictions of the RRKM theory.

A. Binding energy and threshold effects on the product distribution

Several pieces of experimental evidence point consistently to a binding energy for TRA(*d*₃)-D₂O of 2745 cm⁻¹ < *D*₀ < 2869 cm⁻¹ and for the TRA-H₂O binding energy of *D*₀ < 2872 cm⁻¹.

1. Steep rate dependence on energy

First, there is a dramatic isotope effect to the collision-free dissociation rate at threshold. Recall that TRA(*d*₃)-D₂O has a dissociation lifetime of τ_{diss} = 192 ± 51 ns at 2869 cm⁻¹

TABLE III. Calculated RRKM rates compared to experimental rates.

Complex	Excitation energy	Dissociation lifetime	Expt'l. rate (s ⁻¹)	RRKM rate ^a (s ⁻¹)
TRA(<i>d</i> ₃)-D ₂ O	2745 cm ⁻¹ (free OD stretch)	None observed (<5 μs)	<4 × 10 ⁵	...
	2869 cm ⁻¹ (alkyl CH stretch)	192 ± 51 ns	5 × 10 ⁶	6.5 × 10 ³
TRA-H ₂ O	2872 cm ⁻¹ (alkyl CH stretch)	25 ± 3 ns	4 × 10 ⁷	6.2 × 10 ³
	3203 cm ⁻¹ (overtone OH bend)	<8 ns	>1.2 × 10 ⁸	1 × 10 ⁵
	3343 cm ⁻¹ (H-bonded OH stretch)	<8 ns	>1.2 × 10 ⁸	2.1 × 10 ⁵
	3715 cm ⁻¹ (free OH stretch)	<8 ns	>1.2 × 10 ⁸	8 × 10 ⁵

^aValues are taken from the RRKM curve using the binding energies at 2740 and 2840 cm⁻¹ for the H₂O and D₂O, respectively (see text).

excitation energy, while that for TRA-H₂O at 2872 cm⁻¹ is τ_{diss} = 25 ± 3 ns. The most likely cause of this order-of-magnitude increase is simply the change in the binding energy due to zero-point energy effects. Using harmonic vibrational frequencies at the DFT B3LYP/6-31+G*, the binding energy is predicted to be 189 cm⁻¹ greater in TRA(*d*₃)-D₂O than in TRA-H₂O. This steep increase is most easily explained by the 2869/2872 cm⁻¹ excitation energy being very near the threshold, as the dissociation rate is predicted to increase most dramatically with small shifts in the binding energy right near the threshold.

This interpretation is further confirmed by the lack of any signal due to dissociation at 2745 cm⁻¹ despite attempts to observe dissociation with the probe laser moved downstream, where the delay between IR pump and UV probe was ~2 μs. As Table III indicates, we estimate that we should have been able to observe the signal from TRA monomer dissociation products if the complex dissociated with τ_{diss} ≤ 5 μs. Given the small energy difference between the two excitations (2869 and 2745 cm⁻¹), the logical interpretation is simply that the 2745 cm⁻¹ excitation energy is below the dissociation energy for the TRA(*d*₃)-D₂O complex.

2. Internal energy fitting

Second, the TRA monomer products formed following dissociation at threshold have very little internal energy, consistent with an infrared photon of 2869/2872 cm⁻¹ providing the complex with just enough energy to dissociate. The small internal energy is confirmed by the fact that additional energy (Fig. 6) quickly broadens the product signals to the point that no conformation-specific information is achievable in the absence of cooling collisions. Furthermore, a close inspection of the bottom two traces of Fig. 6(b) shows that the TRA(*d*₃, A) product has a narrower product band contour

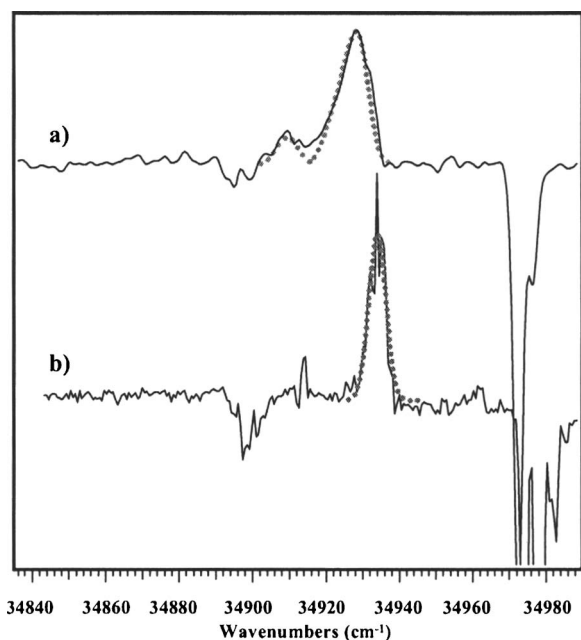


FIG. 8. The IR-UV hole-burning spectra of (a) TRA(A)-H₂O following infrared excitation of the alkyl CH stretch fundamental at 2872 cm⁻¹, recorded under collision free conditions. (b) The analogous scan of TRA(*d*₃,A) from TRA(*d*₃,A)-D₂O excited at 2869 cm⁻¹. The fit in (a) (dotted line) spreads the product population over *v*^{''}=0–3 of TRA(A) and *v*^{''}=0 of TRA(B). The analogous fit in (b) uses population only in *v*^{''}=0 of TRA(*d*₃,A).

under collision-free conditions than TRA(A) from TRA-H₂O. This is consistent with there being less available energy to the products in the former case than in the latter. In addition, no TRA(*d*₃,B) conformer is observed, while there is a small but measurable amount of TRA(B) from TRA-H₂O.

In order to put a more quantitative estimate on the excess energy in the TRA monomer products, we modeled the observed contours to extract information about their vibrational distribution. The Franck-Condon factors associated with the *S*₁ ← *S*₀ transition of TRA monomer greatly favor transitions with Δ*v*=0, so the most likely source of the observed breadth of the bands are sequence bands arising from the low frequency torsions of the ethylamine side chain. In principle, rotational excitation could also contribute to the observed contour; however, the loss of a light H₂O or D₂O from the complex is not expected to result in a very large transfer of angular momentum. Recently, dispersed fluorescence spectroscopy has been used to assign the low frequency torsional structure in a TRA monomer.⁴³ The lowest frequency vibration in TRA is a torsional mode at 44 cm⁻¹ (*S*₀), which becomes 41 cm⁻¹ in *S*₁. We have therefore modeled the observed product contour as a series of sequence bands involving this torsional mode, split off to lower frequency by −3 cm⁻¹ for each succeeding *v*^{''} level. The rotational band contour of each member of the sequence is held fixed at its known shape at that excitation point based on the LIF spectrum recorded under identical conditions.

Figure 8 shows the net result of this fitting for TRA-H₂O [Fig. 8(a)] and TRA(*d*₃)-D₂O [Fig. 8(b)]. In TRA(A) from TRA-H₂O, the band contour of TRA(A) can be fitted with a

distribution spread over *v*^{''}=0–3, while the small population in TRA(B) is consistent with population only present in *v*^{''}=0 of TRA(B). Using the same fitting procedure, the band contour of TRA(*d*₃,A) from TRA(*d*₃)-D₂O [Fig. 8(b)] can be fitted by placing population only in *v*^{''}=0. Using these observations to place maximum internal energies on the dissociating products with $E_{\max}=(v_{\text{obs}}h\nu)$ leads to the following bounds on the binding energies:

$$\text{TRA(A)-H}_2\text{O} \rightarrow \text{TRA(A}, v''=0) + \text{H}_2\text{O},$$

$$D_0 < 2869 - 3 \times 44 = 2740 \text{ cm}^{-1}, \quad (1)$$

$$\text{TRA(A)-H}_2\text{O} \rightarrow \text{TRA(B)} + \text{H}_2\text{O}, \quad D_0 < 2869 \text{ cm}^{-1}, \quad (2)$$

$$\text{TRA}(d_3, \text{A})\text{-D}_2\text{O} \rightarrow \text{TRA}(d_3, \text{A}) + \text{D}_2\text{O},$$

$$2745 < D_0 < 2869 \text{ cm}^{-1}, \quad (3)$$

$$\text{TRA}(d_3, \text{A})\text{-D}_2\text{O} \rightarrow \text{TRA}(d_3, \text{B}) + \text{D}_2\text{O},$$

$$D_0 \geq 2869 \text{ cm}^{-1}. \quad (4)$$

The limit given in Eq. (4) arises from the lack of observable TRA(*d*₃,B) under collision-free and slow-cooling conditions [Fig. 6(b)]. However, the fact that collisions with helium are able to produce TRA(*d*₃,B) under the slightly warmer conditions at *x*/*D*=2.5 [upper trace of Fig. 6(b)] suggests that 2869 cm⁻¹ of excitation energy is very close to the TRA(*d*₃,B) asymptote.

3. Experimental versus computed binding energy

A third piece of evidence that the binding energy is close to the experimentally determined threshold is the consistency of the experimental limits on the binding energy (just derived) with the RIMP2/CBS extrapolated binding energy for TRA-H₂O of 2636 cm⁻¹ (7.53 kcal/mol) and 2825 cm⁻¹ (8.07 kcal/mol) for TRA(*d*₃)-D₂O. These values include ZPE corrections based on the DFT B3LYP/6-31+G* vibrational frequency calculations. As one can see by comparison with Eqs. (1)–(4), the calculated binding energy is in excellent agreement with experiment. In fact, a final consistency check can be made by using the experimental difference in energy between TRA(B) and TRA(A) deduced from the SEP-PT spectra of the TRA monomer of Δ*E*=*E*(TRA(B)) − *E*(TRA(A)) > 126 cm⁻¹.³⁹ One can see that the experimental bounds deduced in the present study [Eqs. (1)–(4)] are consistent with this energy difference. In many ways, the present study is a more accurate measure of these thresholds, particularly in cases such as Eq. (4), where the infrared excitation energy reaches right to the threshold for the process.

B. The observed product quantum yields and the mechanism of dissociation

After establishing bounds on the binding energy of the complex, it is equally important and interesting to consider how the product yields vary with excess energy above threshold. Part of the motivation in doing so is to determine, if possible, whether dissociation occurs directly or whether

other processes, such as isomerization or water shuttling, occur prior to dissociation. The relative yields of A and B are quite sensitive right at threshold. We have just concluded that this sensitivity is a true threshold effect. TRA(A), the lowest energy conformer of TRA, is the only available dissociation channel very near the threshold, while the dissociation channel for TRA(B) lies above and opens up as soon as energetically accessible.

However, it is equally striking that not far above threshold, the product yields are quite insensitive to the amount of excess energy. Over the range 3200–3717 cm^{-1} ; conformers A and B dominate the product distribution with only small contributions from C–F (Fig. 4). This is the case despite the fact that the infrared bands used for excitation involve very different vibrational motions (e.g., H-bonded OH stretch, overtone of OH bend, free OH) and provide excess energies differing by a factor of 2. It is likely that the preference for formation of TRA(A,B) simply reflects the fact that these two products are the lowest energy dissociation product channels. By virtue of this fact, TRA(A) and TRA(B) will be preferred because they have more product states open to them at a given energy than the other, less stable TRA conformers. On the other hand, the presence of these minor products does say something about the competition between dissociation and isomerization. In an earlier study of conformational isomerization in a TRA monomer, many of the energy barriers on the monomer potential energy surface were determined, particularly those separating TRA(A) from wells B–F.³⁹ In particular, the experimental barriers separating conformer A from any of the three anticonformers [C(1), D, and E] are $E_{\text{thresh}} \sim 1300 \text{ cm}^{-1}$ (3.7 kcal/mol), whereas the A \rightarrow B and F thresholds are somewhat lower, in the range $688 < E_{\text{thresh}} < 748 \text{ cm}^{-1}$. Since the maximum internal energy in the product is bounded by the total excess energy available to the complex, the tryptamine monomer has at most 975 cm^{-1} (~ 2.8 kcal/mol) of internal energy, which is still below the barriers to isomerization for all the anticonformer products [C(1), D, and E]. Thus, over the entire energy range probed (2470–3715 cm^{-1}), it is not energetically feasible to first dissociate the water molecule and then isomerize. On the other hand, the calculated barriers to isomerization in the presence of the water molecule are about half the binding energy of the complex (see Fig. 1). Therefore, the fractional population appearing in TRA(C-F) must undergo a sequential process in which isomerization occurs prior to dissociation of the water molecule. In order for this to occur, energy flow into the ethylamine side chain must be sufficient to permit isomerization of the TRA molecule within the complex.

The experimental results also provide some insight into the competition between dissociation and water shuttling reactions. One of the striking results of this study was the change in B/A product yields induced by collisions right at threshold [Fig. 6(b)]. We have argued that formation of B in the presence of collisions may be a threshold energy effect due to the slightly larger internal energy of the complex at this early stage in the expansion. However, the magnitude of the observed effect is beyond what one can easily attribute to this threshold energy effect alone. Recall that TRA(A) and

TRA(B) differ from one another by internal rotation of the amino group by 120° from the Gpy(out) to Gpy(up) orientations. If the water molecule were still attached to the amino group when this internal rotation occurs, helium collisions would be required to enhance the internal rotation of both the amino group and water molecule together. This scenario seems unlikely.

Instead, it seems more probable that the water molecule has, in fact, left the amino group prior to dissociation, with the helium collisions facilitating the internal rotation/tunneling between TRA(A) and TRA(B) in the absence of the water molecule. Therefore, following water shuttling and isomerization, dissociation of the water molecule can occur. This pathway is further supported by the 200 ns dissociation lifetime measured for the complex at threshold, a time sufficiently long that motion of the ethylamine side chain and water molecule shuttling can occur prior to dissociation of the water molecule.

The competition between water shuttling and dissociation is reminiscent of the sequential mechanism proposed by Hineman *et al.*¹⁴ and Bernstein¹⁵ to account for the dissociation rates and product distributions formed in the UV photodissociation of 4-ethylaniline (X)₁ clusters ($X = \text{Ar}, \text{N}_2,$ and CH_4). In that case, intramolecular vibrational redistribution (IVR) into the intermolecular modes of the complex was deduced to occur prior to vibrational predissociation. A statistical model was used to fit the vibrational predissociation rates; however, the fits included the binding energy as a parameter, unlike the present work.^{14,15} We turn now to a similar comparison with statistical theory in TRA-H₂O.

C. Comparison of the measured dissociation rates with RRKM theory predictions

The experimental measurements of the dissociation rates of TRA-H₂O and TRA(*d*₃)-D₂O near threshold provide a point of direct comparison with the predictions from statistical theories for the process. According to RRKM theory, the rate of dissociation at a total internal energy E^* is

$$k(E^*) = \frac{W(E^\ddagger)}{h\rho(E^*)},$$

where $W(E^\ddagger)$ is the number of vibrational states accessible to the transition state with excess energy $E^\ddagger = E^* - E_0$, $\rho(E^*)$ is the density of states of the reactant at energy (E^*), and h is Planck's constant. At threshold, where only a single transition state level is accessible, $W(E^\ddagger) = 1$ and $k(E^*) = 1/h\rho(E^*)$. The dissociation energy for the complex, E_0 , was taken to be 2740 and 2840 cm^{-1} for TRA-H₂O and TRA(*d*₃)-D₂O, respectively [see Eqs. (1)–(4)].

Calculating RRKM rate constants for loose transition states, such as unimolecular dissociation, requires locating the minimum flux configuration because the transition state is not associated with a saddle point in the potential energy surface dividing the reactant and products.¹⁷ In the case of TRA-H₂O the intrinsic reaction coordinate for dissociation was explored starting from its initial optimized geometry. The distance between the pyrrole ring and the water complex was incremented in 0.1 Å steps, with a partial optimization

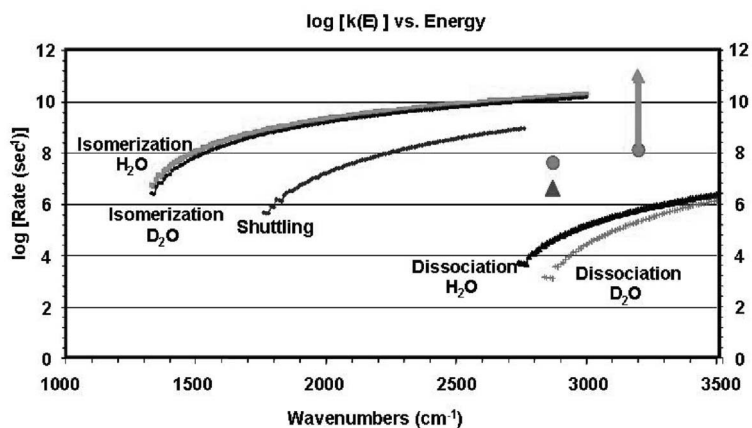


FIG. 9. Calculated RRKM rates for the three competing processes of complex dissociation, water shuttling, and isomerization, compared to the experimentally determined dissociation rates. The experimental isomerization rate for both the deuterated at 2869 cm⁻¹ (triangle) and protonated (circles) species at 2872 and 3208 cm⁻¹ is presented. The experimental dissociation rate at 3208 cm⁻¹ is a lower bound (arrow) since the rise time of the monomer product signal is laser pulse width limited (<8 ns). The dissociation RRKM curves use the binding energies determined from Eqs. (1)–(4) of 2740 and 2840 cm⁻¹ for the H₂O and D₂O, respectively. Note that the experimental rates are two to three orders of magnitude greater than the RRKM predictions.

and normal mode analysis at the B3LYP/6-31+G* level carried out at each step. The direct count method using the unscaled vibrational frequencies at each increment was used to compute the sum of states. The structure with the minimum sum of states corresponds to the location of minimum flux through phase space and is defined as the transition state for the dissociation process.¹⁷ These computations were carried out for the deuterated species as well. RRKM rate constants were calculated using the structures exhibiting the minimum flux through phase space at each excitation energy. The White-Rabinovitch direct count method¹⁷ was used to compute $\rho(E^*)$ and $W(E^*)$ as a function of E^* using harmonic vibrational frequencies for the reactant and transition state. Similar calculations were carried out for the energy-dependent rate constants for representative isomerization and water shuttling reactions using the transition states pictured in Fig. 1.

The results of these calculations, presented in Fig. 9, provide several important predictions with which experiment can be compared. First, as expected, the rates of isomerization and water shuttling are predicted to be much faster than that for dissociation. This is consistent with the deductions in the previous section that isomerization and water shuttling occur prior to loss of the water molecule near the threshold. Second, the experimental rates of dissociation (shown as single data points in Fig. 9) are about three orders of magnitude faster than the RRKM predicted rates (Table III). Third, the very fact that competing processes can occur highlights the fact that a full calculation of the dissociation should not treat dissociation, isomerization, and water shuttling as independent processes, but as competing pathways that must all be included before an accurate prediction for the dissociation rate can be made. Carrying out such a calculation is a daunting task indeed. The full set of minima on the complex's potential energy surface is roughly the multiplicative result of the number of ethylamine side chain minima (27 low-lying minima in TRA monomer) and the number of minima for the water molecule (e.g., NH₂ site, indole NH site, indole π cloud). Furthermore, at these energies, water can traverse over the entire surface of the TRA molecule, exploring large regions of phase space far from any minima and poorly described by any harmonic vibrational levels fixed around a given minimum. Such a calculation is a challenge for future theoretical work. However, the anticipated effect of such a

calculation will be to slow the effective dissociation rate from the harmonic calculation presented in Fig. 9, not to speed it up.

We are left, then, to address possible reasons for this discrepancy between experiment and statistical predictions. One intriguing aspect of the comparison is that the experimental rate is faster than RRKM predictions, not slower. One normally associates non-RRKM behavior with restricted energy flow into the reaction coordinate, leading to a decrease in the time scale for reaction. However, whether restricted energy flow amongst the available states leads to a rate faster or slower than RRKM (where all available states are sampled with equal probability) depends on the starting point in phase space relative to the transition state. If the initial excitation is localized in a particular portion of the molecule that is more strongly coupled to the reaction coordinate, and other states are spectators that are not sampled, the observed rate would be faster than RRKM prediction. This scenario is at least plausible in the present context, where infrared excitation occurs either in the alkyl CH stretch region of the ethylamine side chain (2869/2872 cm⁻¹) or in the water molecule (OH bend overtone, H-bonded OH stretch, or free OH stretch). Unfortunately, given our nanosecond lasers, we have only two quantitatively accurate rate constant measurements, both at threshold for the particular isotope [2869 cm⁻¹ for TRA(*d*₃)-D₂O and 2872 cm⁻¹ for TRA-H₂O] and both involving excitation of the alkyl CH stretch fundamental.

One limiting case scenario would be that dissociation is a direct process in which the alkyl CH stretch level initially excited is coupled directly to the dissociation continuum. However, direct coupling from $v=1$ of the alkyl CH stretch into the intermolecular stretch of the complex would be predicted by the energy gap law to be extremely inefficient.⁴⁴ Furthermore, this scenario flies in the face of the pieces of evidence just given that isomerization and shuttling reactions occur prior to dissociation.

In the Introduction, we described one of the characteristic features of the vibrational level structure of TRA-H₂O relative to smaller complexes such as the water dimer; namely, the low frequency torsional modes associated with the ethylamine side chain, which are in the same frequency range as the intermolecular modes associated with water vibrating against the TRA molecule. Since the water molecule

TABLE IV. Calculated RRKM rates using the indicated restricted density of states.

Model	Rate at 2800 cm ⁻¹	Lifetime
TRA-water		
Harmonic full DOS	4.12E+03 s ⁻¹	243 μs
Scenario 1: TRA-water w/O ring modes	5.31E+04 s ⁻¹	19 μs
Scenario 2: Ethylamine-water	4.37E+05 s ⁻¹	2.3 μs
Scenario 3: Pathway RRKM calculation	9.08E+06 s ⁻¹	110 ns

is complexed to TRA at the amino group on the end of the ethylamine side chain, one anticipates that energy flows from the alkyl CH stretch into the ethylamine torsions and will quickly be shared with the water intermolecular modes, leading to dissociation. This route could lead to a faster-than-statistical dissociation rate if other vibrational modes of TRA (e.g., those associated with the indole ring) are largely decoupled and spectators to this energy flow. Any decoupling of modes could create “bottlenecks” in regions of the vibrational (or rovibrational) state space separating an active region from a decoupled spectator region. Recently, Carpenter has described the circumstances under which this separation into active and spectator space would play a role in bimolecular reactions.⁴⁵ Even more recently, quantum energy flow theory has been generalized to address circumstances under which bottlenecks in phase space can occur, leading to faster-than-RRKM rates observed in rearrangement reactions.⁴⁶ TRA-H₂O photodissociation might provide another example in which bottlenecks between the “stiff” indole ring vibrations and the soft ethylamine side chain and intermolecular modes could exist.⁴⁷

In order to test the plausibility of such a scenario, we carried out a series of RRKM calculations in which the state density was restricted to various active vibrational subspaces. This series of calculations is summarized in Table IV.⁴⁸ In scenario 1, the normal modes of the TRA-H₂O complex were divided into two subgroups depending on whether they were localized in the indole ring or not, as determined from the frequency and mode character of each vibration (Table S1 in Ref. 48). The density of reactant states was then calculated at threshold using only the ethylamine torsional and intermolecular modes. Not surprisingly, this model predicted a rate more than a factor of 10 faster than the full RRKM density; however, this is still almost a factor of 100 slower than experiment.

In scenario 2, the density of states of the TRA-H₂O complex was taken to be that of the ethylamine-H₂O complex. This eliminates, in addition, the lowest frequency ethylamine vibrations in which the entire side chain rocks against the indole ring. This led to a further increase in rate of a factor of 10.

Finally, in scenario 3, the density of reactant states was restricted still further to those that are calculated to be strongly anharmonically coupled to one another along a set of tiers of levels that connect the alkyl CH stretch to the

intermolecular modes of the complex. In order to make this estimate, we carried out a calculation of the full set of cubic and quartic anharmonic coupling constants for the vibrations of the TRA-H₂O complex. The anharmonic cubic and quartic terms were calculated at the HF/3-21+G* level of theory using the anharmonic algorithms⁴⁹ as employed in G03. Starting from the alkyl CH stretch, we followed a pathway through a set of tiers of levels which consist of levels in near resonance, with large cubic anharmonic coupling constants (>2 cm⁻¹ given in Tables S2 and S3 in Ref. 48). This analysis uncovered a set of fast energy flow pathways from the alkyl CH stretch to the intermolecular modes, which by themselves produce a density of background levels of 3.7×10^3 states/cm⁻¹ at 2800 cm⁻¹, equivalent to a threshold dissociation rate of 110 ns, in rough proximity to the threshold rates measured experimentally.

Clearly, these scenarios are useful only as a guide for our thinking, and prove little beyond the qualitative notion that the ethylamine side chain and its strong coupling to the intermolecular modes may be responsible for the speed-up in dissociation rates relative to RRKM predictions. At the same time, they also point to the need for a more rigorous theoretical analysis and for further experimental measurements of the rates of dissociation at higher energies, where the nanosecond lasers used in the present study could provide only lower bounds. Restricted energy flow could lead to interesting mode-specific changes in the rates, which would be fascinating to see and compare with theory.

VI. CONCLUSIONS

Infrared-ultraviolet hole-filling spectroscopy has been used to study IR-induced dissociation in competition with isomerization in tryptamine·H₂O and tryptamine·D₂O complexes. The conformational product yields and rates of the dissociation of the complex as a function of internal energy over this range have been determined. The observed threshold for dissociation occurred at 2872 cm⁻¹ in tryptamine·H₂O and at 2869 cm⁻¹ in tryptamine·D₂O, with no dissociation occurring on the time scale of the experiment at 2745 cm⁻¹. The dissociation time constants varied from ~200 ns for the 2869 cm⁻¹ band of tryptamine·D₂O to ~25 ns for the 2872 cm⁻¹ band of tryptamine·H₂O. At all higher energies, the dissociation lifetime was shorter than the pulse duration of our lasers (8 ns). At all excitation wavelengths, the observed products in the presence of collisions are dominated by conformers A and B with small contributions from the other minor conformers. Right at threshold tryptamine·D₂O at 2869 cm⁻¹, only conformer A is formed in the absence of collisions with helium, while both A and B are observed in the presence of collisions.

The present study has raised nearly as many questions as it has answered. The propensity for the formation of TRA(A) and TRA(B) at all energies could simply reflect the fact that these two products are the most stable TRA conformers, and hence would be preferred on that basis. However, the selection against the other conformers is substantially more complete than in the population distribution observed in the jet-cooled spectrum of TRA monomer, suggesting that certain

regions of the complex's potential energy surface are not fully explored prior to dissociation, despite having sufficient energy to do so. At the same time, the dissociation rates are significantly faster than the RRKM theory would predict. The typical "rule of thumb" that dissipative IVR begins to proceed at a state density of 10 states/cm⁻¹ is far exceeded at the initial energies where dissociation can occur (10⁶ states/cm⁻¹).^{15,50} Yet, the rate of dissociation is orders of magnitude faster than RRKM predictions. This discrepancy is in keeping with a growing body of evidence that indicates that the rate of conformational isomerization of modest-sized molecules deviates from RRKM predictions due to insufficiently rapid or incomplete energy flow.⁵¹ Full resolution of these issues awaits further input from both theory and experiment.

ACKNOWLEDGMENTS

The authors gratefully acknowledge support for the work from the National Science Foundation (CHE-0242818). One of the authors (J.M.H.) acknowledges start-up funds from The Ohio State University and a start-up allocation from The Ohio Supercomputer Center. Another author (J.R.C.) acknowledges partial support from the Purdue Research Foundation for a Graduate Student Assistantship and Dr. Eugene Myshakin for advice on the anharmonic calculations in G03. Two authors (T.S.Z. and J.R.C.) gratefully acknowledge Professor David M. Leitner for fruitful discussions of IVR, energy flow, and enhanced reaction rates.

¹T. V. Nguyen, T. M. Korter, and D. W. Pratt, *Mol. Phys.* **103**, 1603 (2005).

²Y. R. Wu and D. H. Levy, *J. Chem. Phys.* **91**, 5278 (1989).

³L. A. Philips and D. H. Levy, *J. Chem. Phys.* **89**, 85 (1988).

⁴J. R. Carney and T. S. Zwier, *Chem. Phys. Lett.* **341**, 77 (2001).

⁵J. R. Carney and T. S. Zwier, *J. Phys. Chem. A* **104**, 8677 (2000).

⁶T. S. Zwier, *J. Phys. Chem. A* **110**, 4133 (2006).

⁷J. R. Clarkson, E. Baquero, and T. S. Zwier, *J. Chem. Phys.* **122**, 214312 (2005).

⁸J. R. Clarkson, E. Baquero, V. A. Shubert, E. M. Myshakin, K. D. Jordan, and T. S. Zwier, *Science* **307**, 1443 (2005).

⁹L. A. Peteanu and D. H. Levy, *J. Phys. Chem.* **92**, 6554 (1988).

¹⁰L. L. Connell, T. C. Corcoran, P. W. Joireman, and P. M. Felker, *J. Phys. Chem.* **94**, 1229 (1990).

¹¹T. S. Zwier, *J. Phys. Chem. A* **105**, 8827 (2001).

¹²M. Schmitt, M. Bohm, C. Ratzer, C. Vu, I. Kalkman, and W. L. Meerts, *J. Am. Chem. Soc.* **127**, 10356 (2005).

¹³B. C. Dian, A. Longarte, and T. S. Zwier, *Science* **296**, 2369 (2002).

¹⁴M. F. Hineman, E. R. Bernstein, and D. E. Kelly, *J. Chem. Phys.* **98**, 2516 (1993).

¹⁵E. R. Bernstein, *Annu. Rev. Phys. Chem.* **46**, 197 (1995).

¹⁶R. A. Marcus, *J. Chem. Phys.* **20**, 359 (1952).

¹⁷T. Baer and W. L. Hase, *Unimolecular Reaction Dynamics: Theory and Experiments* (Oxford University Press, Oxford, 1996).

¹⁸B. C. Dian, A. Longarte, P. R. Winter, and T. S. Zwier, *J. Chem. Phys.* **120**, 133 (2004).

¹⁹J. R. Carney, B. C. Dian, G. M. Florio, and T. S. Zwier, *J. Am. Chem.*

Soc. **123**, 5596 (2001).

²⁰R. N. Pribble, C. J. Gruenloh, and T. S. Zwier, *Chem. Phys. Lett.* **262**, 627 (1996).

²¹M. J. Frisch, J. A. Pople, and J. S. Binkley, *J. Chem. Phys.* **80**, 3265 (1984).

²²C. Lee, W. Yang, and R. G. Parr, *Phys. Rev. B* **37**, 785 (1988); A. D. Becke, *Phys. Rev. A* **38**, 3098 (1988).

²³M. J. Frisch, G. W. Trucks, H. B. Schlegel *et al.*, GAUSSIAN03, Revision C.02 (Gaussian, Inc., Wallingford, CT, 2004).

²⁴C. Peng and H. B. Schegel, *Isr. J. Chem.* **33**, 449 (1993).

²⁵S. Grimme, *J. Comput. Chem.* **25**, 1463 (2004).

²⁶S. F. Boys and F. Bernardi, *Mol. Phys.* **19**, 553 (1970).

²⁷M. Schutz, T. Burgi, S. Leutwyler, and T. Fischer, *J. Chem. Phys.* **99**, 1469 (1993).

²⁸F. Weigend and M. Häser, *Theor. Chem. Acc.* **97**, 331 (1997).

²⁹F. Weigend, M. Häser, H. Patzelt, and R. Ahlrichs, *Chem. Phys. Lett.* **294**, 143 (1998).

³⁰R. A. DiStasio, Jr., Y. Jung, and M. Head-Gordon, *J. Chem. Theory Comput.* **1**, 862 (2005).

³¹F. Weigend, A. Köhn, and C. Hättig, *J. Chem. Phys.* **116**, 3175 (2002).

³²Y. Shao, L. F. Molnar, Y. Jung *et al.*, *Phys. Chem. Chem. Phys.* **8**, 3172 (2006).

³³R. A. DiStasio, Jr., R. P. Steele, Y. M. Rhee, Y. Shao, and M. Head-Gordon, *J. Comput. Chem.* (in press).

³⁴A. Halkier, T. Helgaker, P. Jorgensen, W. Klopper, H. Koch, J. Olsen, and A. K. Wilson, *Chem. Phys. Lett.* **286**, 243 (1998).

³⁵M. Schmitt, R. Brause, C. M. Marian, S. Salzmann, and W. L. Meerts, *J. Chem. Phys.* **125**, 124309 (2006).

³⁶P. Salvador, S. Simon, M. Duran, and J. J. Dannenburg, *J. Chem. Phys.* **113**, 5666 (2000); W. Zheng, W. Wang, X. Pu, A. Tian, and N. B. Wong, *J. Mol. Struct.: THEOCHEM* **631**, 171 (2003).

³⁷D. Moran, A. C. Simmonett, F. E. Leach, W. D. Allen, P. V. R. Schleyer, and H. F. Schaefer, *J. Am. Chem. Soc.* **128**, 9342 (2006).

³⁸W. Caminati, *Phys. Chem. Chem. Phys.* **6**, 2806 (2004).

³⁹J. R. Clarkson, B. C. Dian, L. Moriggi, A. DeFusco, V. McCarthy, K. D. Jordan, and T. S. Zwier, *J. Chem. Phys.* **122**, 214311 (2005).

⁴⁰S. M. Bellm and W. D. Lawrance, *J. Chem. Phys.* **118**, 2581 (2003).

⁴¹Using an estimated TRA-He cross section of 200 Å² and a backing pressure of 8 bar helium, we can estimate the total number of TRA-He collisions in the supersonic expansion as the complexes traverse the distance between IR excitation ($x/D=2.5$) and LIF detection ($x/D=6$). The highest collision rate occurs at $x/D=2.5$, where complex-He collisions occur on the 250 ps time scale.

⁴²D. A. Evans, D. J. Wales, B. C. Dian, and T. S. Zwier, *J. Chem. Phys.* **120**, 148 (2004).

⁴³M. Schmitt, K. Feng, M. Bohm, and K. Kleiner, *J. Chem. Phys.* **125**, 144303 (2006).

⁴⁴G. E. Ewing, *J. Phys. Chem.* **91**, 4662 (1987).

⁴⁵B. K. Carpenter, *Annu. Rev. Phys. Chem.* **56**, 57 (2005).

⁴⁶D. M. Leitner and P. G. Wolynes, *Chem. Phys.* **329**, 163 (2006).

⁴⁷D. M. Leitner (private communication).

⁴⁸See EPAPS Document No. E-JCPSA6-126-007712 for Tables S1, S2, and S3 that include vibrational modes and frequencies used for the RRKM rate calculations. This document can be reached via a direct link in the online article's HTML reference section or via the EPAPS homepage (<http://www.aip.org/pubservs/epaps.html>).

⁴⁹V. Barone, *J. Chem. Phys.* **122**, 014108 (2005); **120**, 3059 (2004).

⁵⁰R. Knochenmuss, V. Karbach, C. Wickleder, S. Graf, and S. Leutwyler, *J. Phys. Chem. A* **102**, 1935 (1998).

⁵¹J. K. Agbo, D. M. Leitner, D. A. Evans, and D. J. Wales, *J. Chem. Phys.* **123**, 124304 (2005); R. Bigwood and M. Gruebele, *Chem. Phys. Lett.* **235**, 604 (1995); R. Bigwood, M. Gruebele, D. M. Leitner, and P. G. Wolynes, *Proc. Natl. Acad. Sci. U.S.A.* **95**, 5960 (1998).